Anal. Bioanal. Electrochem., Vol. 9, No. 3, 2017, 374-389

Analytical & Bioanalytical Electrochemistry

2017 by CEE
www.abechem.com

Full Paper

Electrochemical Corrosion Studies of Zn-CuO and Zn-NiO-CuO Composite Coatings on Mild Steel

Kallappa Deepa, Thimmappa Venkatarangaiah Venkatesha,* Chandrakanth Nagaraja and Mutugadahalli Rangaswamy Vinutha

Department of Studies in Chemistry, School of Chemical Sciences, Kuvempu University, Shankaraghatta-577451, Shimoga, Karnataka, India

*Corresponding Author, Tel.: +91 9448855079; Fax: +91 08282 256255

E-Mail: drtvvenkatesha@yahoo.co.uk

Received: 20 March 2017 / Received in revised form: 21 April 2017 / Accepted: 4 May 2017 / Published online: 15 May 2017

Abstract- Copper oxide and nickel oxide-copper oxide (NiO-CuO) metal oxide nanoparticles were prepared by co-precipitation method in aqueous solution using sodium hydroxide as precipitating agent and Cetyl Trimethyl Ammonium Bromide (CTAB) as a surfactant. The particles were characterized by XRD, SEM, EDS and FTIR analysis. The crystallite sizes of both metal oxide particles were in the nano range calculated by Debye-Scherrer equation. The prepared metal oxide nanoparticles were employed for the fabrication of zinc-composite coating on mild steel by electroplating and their corrosion behaviour was investigated by Tafel and Electrochemical impedance spectroscopy in corrosive media of 3.5% NaCl solution. The surface morphology of coated steel articles and also their corrosion morphology have been characterized by scanning electron microscopic (SEM) images.

Keywords- NiO-CuO nanoparticles, Zn-composite coating, Corrosion, Electrochemical impedance spectroscopy, Tafel

1. INTRODUCTION

Zinc (Zn) electroplated steel materials have found widespread applications in industries due to their good corrosion resistance property. Zn coating has been using since a long time to provide sacrificial protection for steel against corrosion. The zinc film on steel has been

applied by various techniques including hot dipping, cladding and electrodeposition [1-3]. However, the formation of white rust on the zinc surface causes white rust corrosion of zinc coating thereby affect the service life of the coated steel material. White rust formation can be effectively controlled through chrome passivation on the surface of the zinc but, the chromium salts are toxic in nature. Even though zinc after passivation with chrome provides excellent protection but electroplated zinc alloys and composite coatings without chrome passivation have been developed for a better performance against corrosion in similar applications. The development of good composite coating which exhibits excellent service life under a corrosive atmosphere at lower thickness is in great demand than the conventional zinc coatings [4-6]. Nowadays Zn coating and Zn alloy coating on steel materials with the addition of a minute quantity of nanoparticles in Zn matrix during coating have received attention because of the improved corrosion resistance property compare to pure Zn coating. The lifespan of the Zn coated steel materials can be enhanced by good Zn-nanocomposite coatings which exhibit greater potential properties such as thermal stability, wear resistance, and corrosion resistance. These properties are achieved through the incorporation of certain metal oxides such as TiO_2, SnO_2, NiO, Al_2O_3, ZrO_2, CeO_2, CuO etc [7-9]. The TiO_2 nanoparticles were used in the preparation of Zn composite coating for corrosion studies by many authors [10]. The TiO_2 nanoparticles were successfully incorporated into Zn coating [6]. Anatase and rutile phase TiO_2 nanoparticles were used for Zn-TiO_2 composite coating on mild steel and the results indicated better corrosion protection over Zn-coating [11]. The SnO_2 nanoparticles in the Zn-composite coating showed excellent wear resistance, hardness and corrosion resistance properties [12]. The Zn-ZrO_2 composite coating on mild steel provided better corrosion resistance and wear resistance [13]. The inclusion of CeO_2 nanoparticles into the Zn matrix improved the corrosion resistance of mild steel [14]. NiO nanoparticles generated by solution combustion method were used to enhance the corrosion resistance property of Zn coating, the deposit exhibited good corrosion resistance [15]. Similarly, the Zn-alloy coating with the inclusion of metal oxide nanoparticles has been also studied by researchers for the better service life of Zn coating on steel. Zn-Ni-SiO_2 composite coating exhibited very good corrosion resistance than Zn-Ni alloy coating on mild steel [16]. The electrochemically synthesized hexagonal shaped CuO nanoparticles were incorporated into Zn-Ni alloy matrix and the corrosion performance has been studied by Chandrappa et al. and the results showed excellent corrosion resistance property [17]. Nowadays single metal oxides have been replaced by mixed metal oxides in composite coating field due to significant improvement in their chemical and physical properties. Because mixed metal oxides have remarkable properties and advanced technological applications compare to single metal oxides. In this way many investigations have been carried out by researchers, the Zn-Cr_2O_3-SiO_2 composite coating on mild steel was investigated for better tribological and corrosion resistance [18]. Composite coatings of Zn-Al_2O_3-SiC and Zn-ZnO-Y_2O_3 were

studied for better corrosion resistance performance on mild steel [19-20]. The CuO and NiO nanoparticles possess greater catalytic activity, large surface area, excellent chemical stability and photochemical activity [15,17]. Present work gives the preparation of CuO, mixed NiO-CuO nanoparticles and fabrication of Zn-CuO and Zn-NiO-CuO composite coating on mild steel. The prepared composite coatings were used to analyze their corrosion behaviour in NaCl solution. CuO and NiO-CuO nanoparticles were prepared by co-precipitation method and characterized by FTIR, XRD, SEM and EDS analysis. Corrosion behavior of the coatings was investigated by using electrochemical techniques such as Tafel and Electrochemical impedance spectroscopy.

2. EXPERIMENTAL SECTION

2.1. Materials and Methods

Copper(II)acetate monohydrate, Nickel(II)chloride hexahydrate and Sodium hydroxide were purchased from Himedia-AR, Mumbai, India. AR grade CTAB was purchased from LOBA Chemie Laboratory reagents and fine chemicals-Mumbai, India. Above chemicals were used as received without further purification. All the experiments were carried out using Millipore water (Sp.resistance-15 mΩ at 25 $^{\circ}$C, Millipore Elix-3 water purification system, France).

2.2. Synthesis and characterization of CuO and NiO-CuO nanoparticles

The CuO and mixed NiO-CuO nanoparticles were prepared by co-precipitation method. The CuO nanoparticles have prepared by dissolving $Cu(Ac)_2.H_2O$ (0.1 M) and CTAB (5 mM) in 100 ml water. The pH of this solution was raised to 9 by the dropwise addition of dilute NaOH and stirred for 2 h at room temperature. The obtained precipitate of CuO was allowed to settle for an hour and then filtered. The precipitate was washed several times with water, followed by absolute ethanol. The product was dried overnight at 80 ^{o}C in an oven and finely ground in an agate mortar. The grounded sample was calcined for 2 h at 500 ^{o}C in a Muffle Furnace. Similar procedure was adopted for the preparation of mixed NiO-CuO nanoparticles, in which $NiCl_2.6H_2O$ (0.02 M) and $Cu(Ac)_2.H_2O$ (0.1 M) were dissolved in 100 mL water along with CTAB (5 mM). The prepared nanoparticles were characterized by using XRD, SEM and FTIR spectroscopy.

Powder X-ray diffraction studies of synthesized nanoparticles were carried out in PANalytical X'pert pro powder diffractometer with CuKα (λ=1.5418Å). FT-IR spectrometer (Bruker) was used to identify the modes of bending and stretching vibration of functional groups and metal-oxygen bonds. The surface morphological images of nanoparticles before coating and metal samples after fabrication were obtained by scanning electron microscopic

(SEM) technique using Hitachi instrument (Japan). The elemental composition of the nanoparticles was examined by energy dispersive spectroscopic (EDX) studies.

2.3. Fabrication and electrochemical corrosion studies of Zn, Zn-CuO and Zn-NiO-CuO coatings

The basic bath composition for zinc electroplating is given in Table 1(a). For Zn-CuO and Zn-NiO-CuO composite coating preparation, the bath composition as in table 1(b) and (c) were used respectively. The steel plates (40×40×1 mm) were polished mechanically using different grits of emery papers and degreased in acetone then washed in distilled water and used as cathodes. Zinc metal plate with the same dimension of steel plate was used as an anode and it was dipped in 5% HCl for few seconds to activate the surface followed by water wash before placing in electrolyte solution. Hull cell experiment was conducted at cell current 2A using bath solution given in Table 1(a). The hull cell plate showed good deposit between current density 0.2 A/dm^2 to $7A/dm^2$. Thus for electroplating experiments, the current density $3A/dm^2$ was employed. The pH of the bath solution was maintained as 3.5 by the addition of dilute H_2SO_4. Before electroplating of Zn-CuO and Zn-NiO-CuO composite coatings, the respective bath solutions were stirred for 5 h. The deposition of Zn and Zn-composite films on mild steel has been carried out for the duration of 10 min at 300 rpm.

The deposits were subjected to corrosion studies in 3.5% NaCl solution. The Tafel and Electrochemical impedance spectroscopy techniques were carried out to analyze the corrosion behavior of coatings using CHI660C Electrochemical workstation (USA make). The conventional three-electrode cell was employed for electrochemical measurement with an electrodeposited steel plate (1×1 cm^2), platinum wire and saturated calomel electrode (SCE) as working, counter and reference electrode respectively.

Table 1. Bath composition and operating parameters of **(a)** Zn (**b)** Zn-CuO **(c)** Zn-NiO-CuO

	Bath constituents	**Operating parameters**
1(a)	$ZnSO_4$- 200g/L Na_2SO_4-50g/L NaCl-20g/L H_3BO_3-12g/L SLS-0.5g/L	Anode: zinc plate (99.99% pure) Cathode: mild steel plate Current density: 3 A/dm^2 Plating time: 10 min Stirring speed: 300 rpm pH: 3.5 Temperature: 303K
1(b)	1(a) + CuO-1g/L	
1(c)	1(a) + NiO-CuO 1g/L 1(a) + NiO-CuO 2g/ 1(a) + NiO-CuO 3g/L	

3. RESULTS AND DISCUSSION

3.1. Characterization of CuO and NiO-CuO nanoparticles

3.1.1. XRD studies

Structural properties of CuO and mixed NiO-CuO nanoparticles were studied by XRD analysis. XRD spectra revealed that the nanoparticles were well crystallized with monoclinic CuO phase (space group C2/c). The major duel peaks at 002 and 111 planes appeared in both CuO and mixed NiO-CuO nanoparticles indicated the presence of monoclinic phase of CuO.

The appeared diffraction planes of miller indices were well matched with standard JCPDS (45-09357) of CuO. The ionic radius of Ni^{2+} is 0.69Å and is closer to the ionic radius of Cu^{2+}(0.73Å) hence there is no much variation in the lattice parameters of NiO-CuO compare to pure CuO Nanoparticles [21]. The 2θ value of secondary diffraction peaks at 43Å and 37Å in NiO-CuO nanoparticles diffraction pattern are due to NiO phase [22-25]. The crystallite size was calculated by Debye-Scherrer formula,

$$D = \frac{K\lambda}{\beta Cos\,\theta} \quad (1)$$

Where D is the diameter of the crystallite size, K is the shape factor (0.9), λ is the wavelength of radiation source used, β is the angular peak width at half maximum intensity (FWHM) and θ is the Bragg's angle. The calculated average crystallite sizes of the pure CuO and NiO-CuO nanoparticles were found to be 34.75 nm and 20.40 nm respectively.

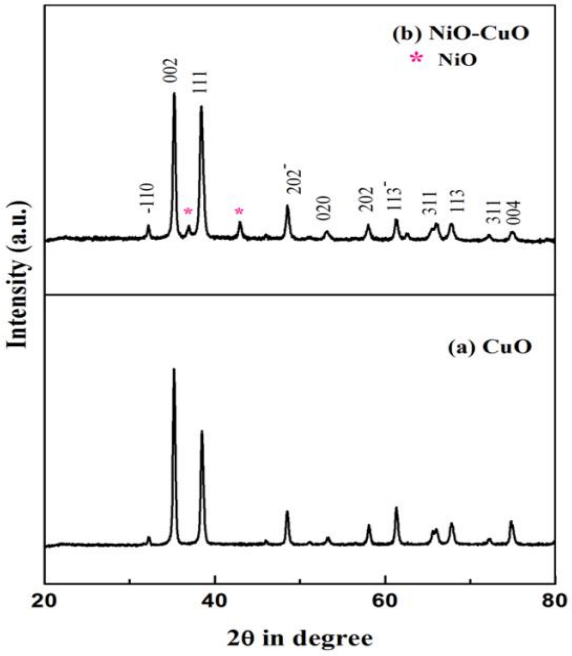

Fig. 1. XRD Pattern of (a) CuO and (b) NiO-CuO nanoparticles

3.1.2. SEM with EDS analysis

The SEM images of CuO and mixed NiO-CuO nanoparticles were depicted in Fig. 2(a) and Fig. 2(b).

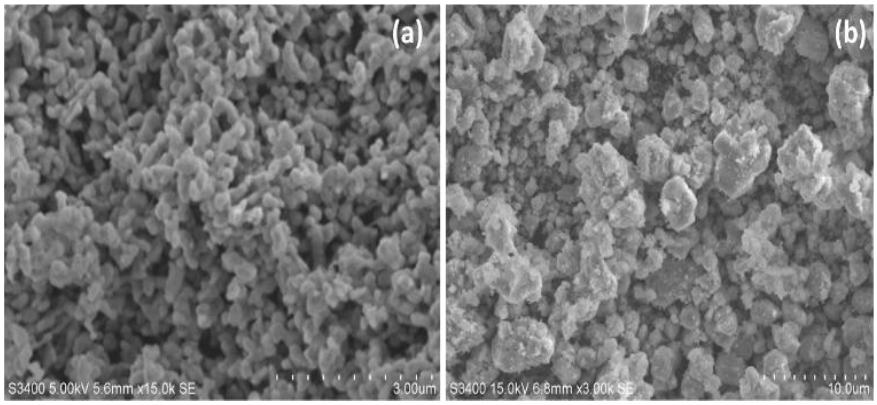

Fig. 2. SEM images of (a) CuO and (b) NiO-CuO nanoparticles

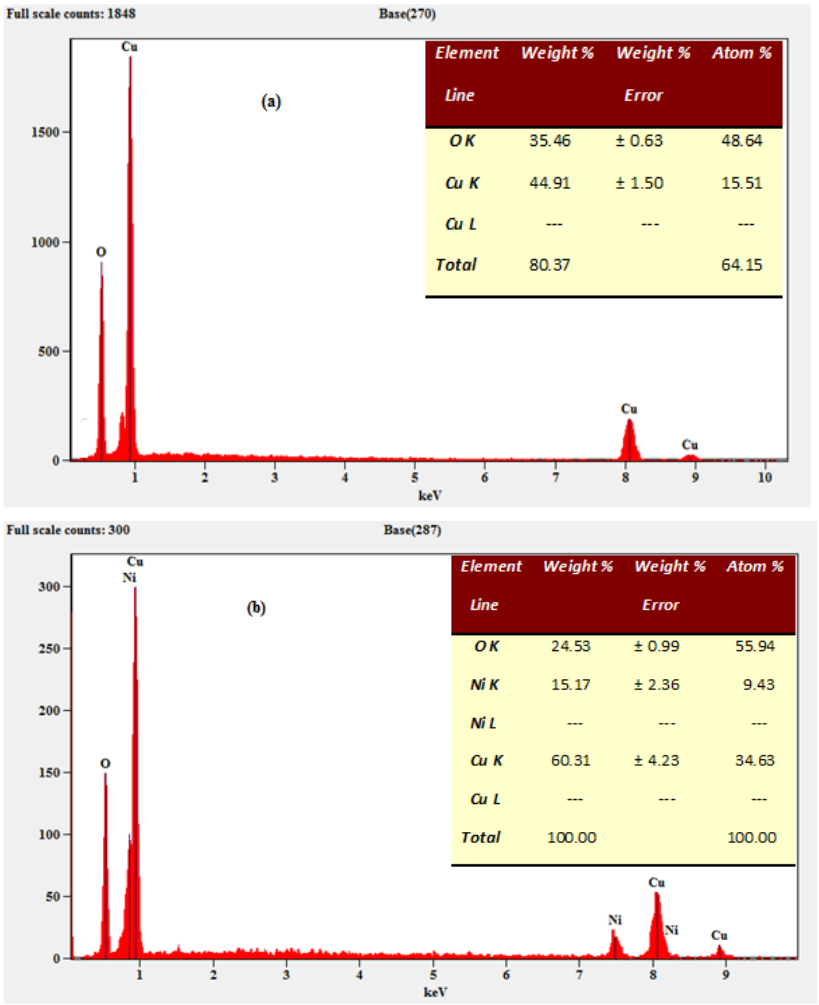

Fig. 3. EDS spectra and atomic percentage of constituent elements (a) CuO (b) NiO-CuO

The morphology of CuO in Fig. 2(a) shows the formation of small spindle-shaped particles. Preparation of a mixed NiO-CuO affects the morphology of spindle shape changed into agglomerated spherical structure. EDS inspection of CuO in Fig. 3(a) indicates the presence of Cu and O elements in CuO nanoparticles and percentage composition of the constituents. Similarly, Fig. 3(b) showed the composition of Ni, Cu and O elements and also the percentage of the composition. The results indicate the nanoparticles were free from foreign impurities.

3.1.3 FTIR studies

Functional groups adsorbed during the preparation of the nanoparticles were analyzed by Fourier Transform infrared spectral investigation. Both the samples CuO and NiO-CuO nanoparticles showed absorption peak at 3419 cm^{-1} was due to –OH stretching vibration and peak at 1632.72 cm^{-1} due to –OH bending vibration of water molecules. The characteristic peaks appeared at 595.53, 503.72, 445.54, and 408.02 cm^{-1} corresponds to stretching vibrations of monoclinic CuO. The strong absorption band at 503.72 cm^{-1} was due to Cu-O stretching mode [21-28]. The absorption peaks observed at 1123.05 and 1045.17 cm^{-1} in NiO-CuO nanoparticles are due to the O-C=O symmetric and asymmetric stretching vibrations [21].

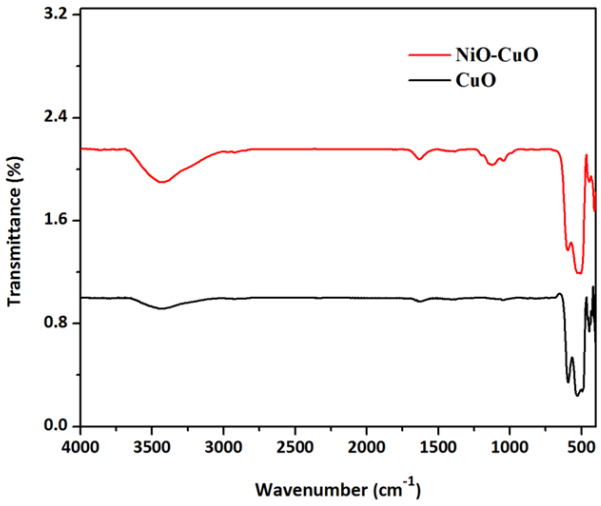

Fig. 4. FTIR spectra of CuO and NiO-CuO nanoparticles

3.2. Corrosion studies of the fabricated coatings

3.2.1. OCP measurement

When a metallic species is subjected to the corrosive medium, metal dissolution occurs on its surface through electrochemical reactions, the metal surface attains a constant potential and thus reach the equilibrium condition (rate of redox process was equal) under which no

net current flows in the system referred as open circuit potential (OCP). The OCP with a variation of time in 3.5% NaCl for the Zn, Zn–CuO(1 g/L) and Zn-NiO-CuO(2 g/L) is shown in Fig. 5. In the beginning, OCP for Zn and Zn-composite coatings was -1.091, -1.089 and -1.083 V with reference to the SCE respectively. The coatings reached equilibrium state after 2 h and acquire potential of -1.109, -1.094 and -1.088 V *vs*. SCE respectively shown in Fig. 5. The pure zinc coating showed more negative potential whereas Zn-NiO-CuO composite coating attained less negative potential than the Zn-CuO composite coating. The OCP measurement depicted that the Zn-composite coating by NiO-CuO nanoparticles exhibited more stable character than CuO and pure Zn coating on mild steel.

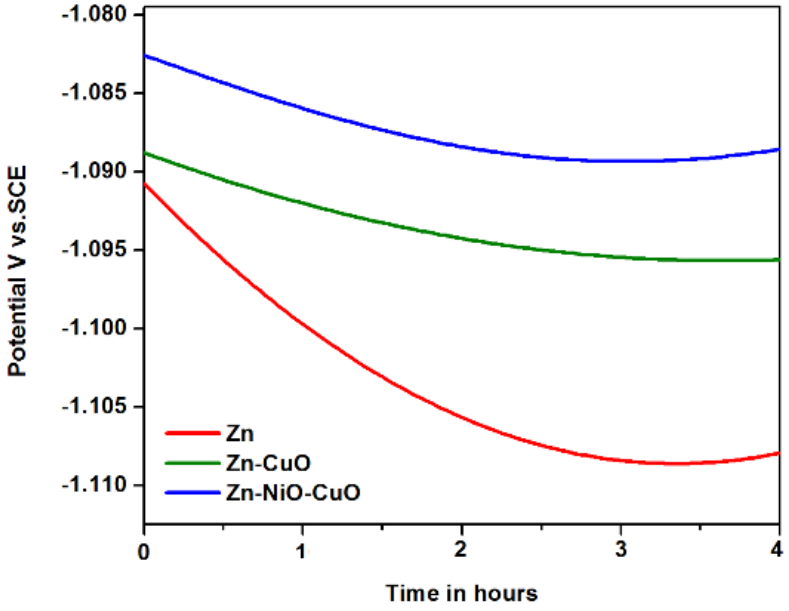

Fig. 5. OCP of (a) Zn coating (b) Zn-CuO (c) Zn-NiO-CuO

3.2.2. Corrosion rate measurement by Tafel method

Corrosion behaviour of electroplated specimens was studied by Tafel polarization performed in corrosive media of 3.5% NaCl solution. The coated materials were immersed in NaCl solution to attain OCP and the polarization data such as, corrosion current (I_{corr}), corrosion potential (E_{corr}), corrosion rate and polarisation resistance (Rp) were collected at a scan rate of 0.01 V/s. Corrosion rate (CR) of the coatings has been calculated by the following equation.

$$CR(mpy) = \frac{0.13 Icorr\ (Eq.wt)}{d} \qquad (2)$$

Where, Eq. wt. is the equivalent weight and d is the density of the zinc metal in g/cm^3. The corrosion parameters were tabulated in Table 2. The results indicated that the corrosion

potential E_{corr} for pure Zn coating was more negative (-1.138 V) and it was shifted towards less negative potential (-1.121 and -1.081 V) for Zn-CuO and Zn-NiO-CuO composite coatings as shown in the Fig. 6. It is because of the higher chemical stability of composite coating induced by incorporation of nanoparticles in Zn matrix attained more passive nature compares to pure zinc coating and hence I_{corr} value was lesser for composite coating than the pure zinc coated sample. From the obtained results it could be observed that compare to CuO, the presence of NiO-CuO nanoparticles in zinc matrix enhanced the corrosion resistance property of Zn coated steel due to smaller size of NiO-CuO nanoparticles which created more nucleation sites than CuO nanoparticles and decreased the grain size of the surface thus resulted in the formation of the more uniform passive surface.

Table 2. Corrosion parameters of the coatings derived from Tafel plots

Samples	**E_{corr} (V)**	**$I_{corr}\times10^{-5}$**	**β_c**	**β_a**	**LP (Ωcm^2)**	**Corrosion rate$\times10^{-5}$ (g/h)**
Zn coated	-1.138	6.703	6.903	20.879	234	6.984
Zn-1g/L CuO	-1.121	3.879	5.071	15.461	546	4.040
Zn-1g/L NiO-CuO	-1.114	3.328	5.820	15.263	620	3.467
Zn-2g/L NiO-CuO	-1.081	1.816	6.362	18.895	948	1.845
Zn-3g/L NiO-CuO	-1.089	3.050	2.671	13.621	875	3.177

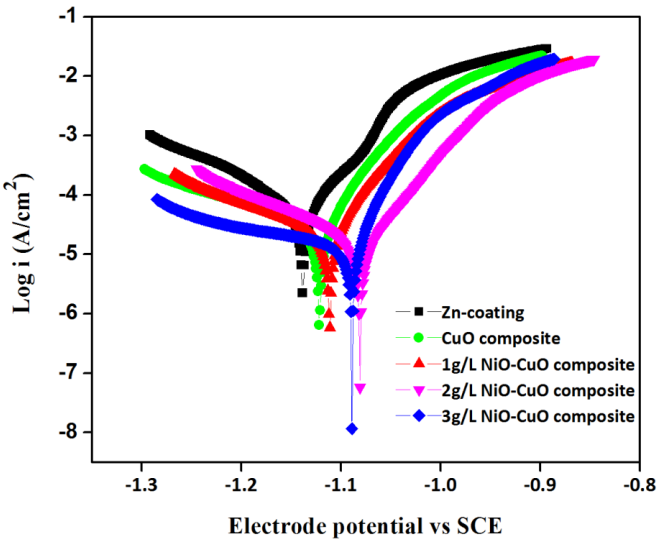

Fig. 6. Polarization curves for Zinc and Zn-composite coatings in 3.5% NaCl solution

The corrosion resistance property of Zn-composite coating obtained at 2 g/L of NiO-CuO is higher than the composite at 3 g/L probably due to poor adhesion of nanoparticles [29-34].

3.2.3. Electrochemical impedance spectroscopic (EIS) studies

The corrosion resistance property of the steel substrates coated with Zn and Zn-composite coatings was investigated by electrochemical impedance analysis in 3.5% NaCl solution. The EIS has been explained on the basis of metal dissolution in the form of redox process with respect to the OCP. Fig. 7, 9 and 10 show the impedance measurement in the form of Nyquist and bode plots of the prepared coatings recorded in the frequency range from 0.1 Hz to 10 kHz with ±5 mV AC amplitude respectively. Nyquist plots were displayed as imaginary part of the impedance *vs* real part and bode plots were presented as phase angle and modulus of the impedance as a function of frequency. The Nyquist plots were matched with an equivalent circuit using Z-simp win 3.21 software. The Fig.8 shows the well fitted equivalent circuit model for the Nyquist plots. The circuit is composed of solution resistance (Rs), the coating resistance (R_{coat}), charge transfer resistance (R_{ct}), constant phase element (CPE) for coating (Q_{coat}) and CPE for double layer capacitance (Q_{dl}). The presence of CPE symbolizes that the nonideal capacitance behavior of the working electrode due to inhomogeneity of the surface. The impedance offered by CPE is given by the following equation:

$$ZCPE = Y_0^{-1} (i\omega)^{-n} \quad (3)$$

Where, Y_0 is CPE constant, i^2=-1, an imaginary number, ω is angular frequency and n denoted the exponent of CPE used to denote the micro roughness, porosity and inhomogeneity of the metal surface. The C_{dl} of CPE was calculated using the following equation.

$$C_{dl} = (QRct^{1-n})^{1/n} \quad (4)$$

The R_{coat} and Q_{coat} represent coating resistance and capacitance of the working electrode. The increased coating resistance (R_{coat}) value for Zn-composite coatings was due to fewer pores on the surface compare to pure zinc coated steel plate. The increased porosity on coating surface permits the electrolyte solution to contact with coated material thereby increases the risk of corrosion product formation. The Q_{dl} represents the double layer capacitance of the electrode and electrolyte solution. The lower Q_{dl} value of Zn-NiO-CuO composite coating indicated that the more stability of the coated surface towards corrosive environment than the Zn-CuO and pure zinc coating. R_{ct} value was ascribed to the redox process taking place due to the formation of a corrosion product.

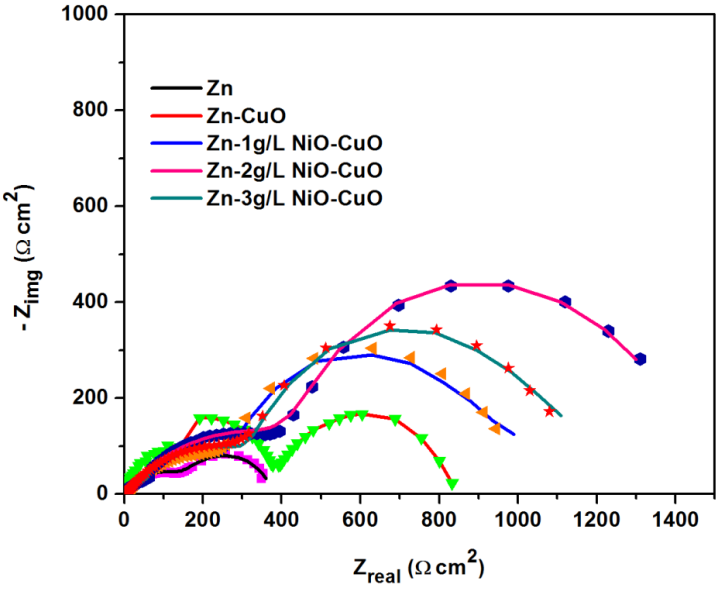

Fig. 7. Nyquist plots of Zn and Zn-composite coatings experimental (-) and symbol equivalent circuit fitted

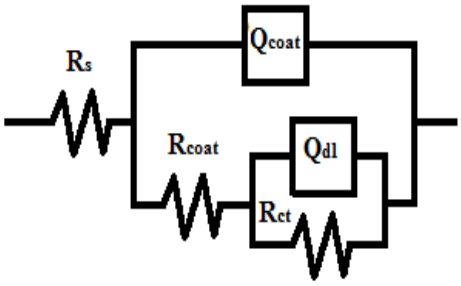

Fig. 8. Equivalent circuit model for Zn and Zn-composite coatings

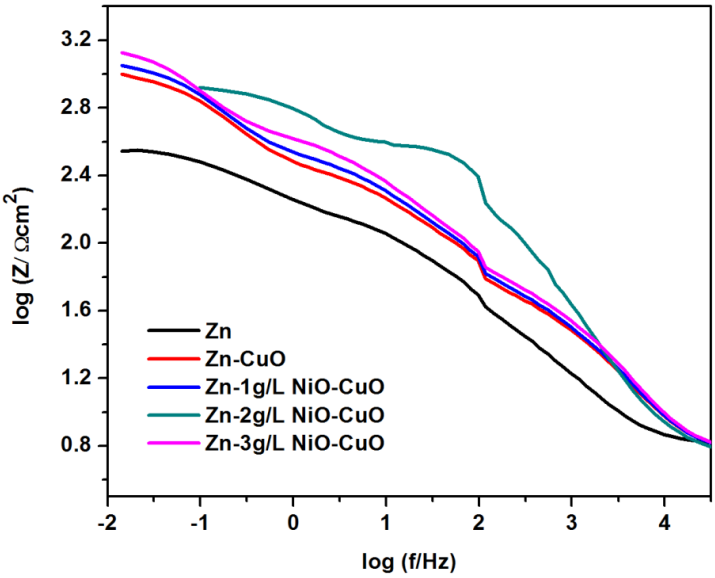

Fig. 9. Bode plots of Zn and Zn-composite coatings

The lower the charge transfer resistance signify that the formation of a thin layer corrosion product on the electrode surface. Zn-NiO-CuO composite coating exhibited good Corrosion resistance behaviour at 2 g/L. Further increased the concentration of nanoparticles to 3 g/L decreased the impedance of the coating. The increased concentration of nanoparticles leads to agglomeration and probably poor adhesion was takes place hence the coating corrosion resistance property decreased gradually. The investigated impedance parameters were recorded in Table 3. The polarization resistance (R_P) was calculated by the sum of the resistances R_{coat} and R_{ct}. R_P value was greater for Zn-NiO-CuO composite coating compared to Zn-CuO and pure zinc coating. A similar trend has been followed in bode plots that the higher modulus impedance and maximum phase angle observed for Zn-NiO-CuO(2g/L) coating indicated that the more homogeneous surface with good corrosion resistance property [35-38].

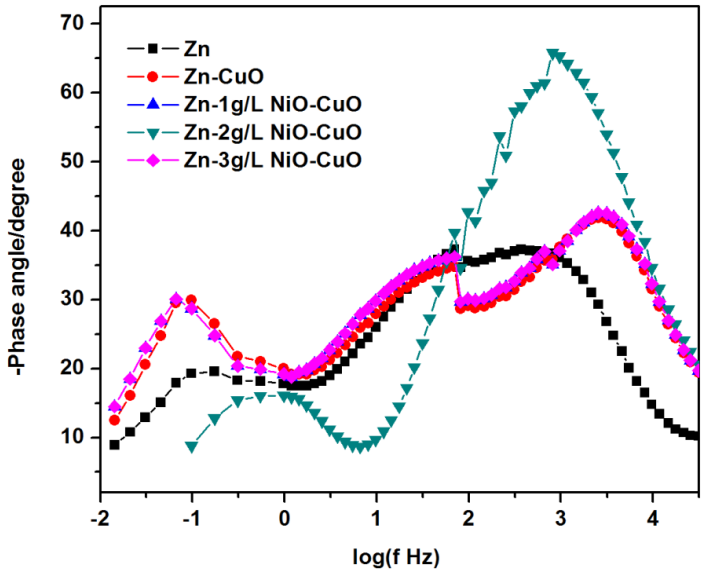

Fig. 10. Bode phase angle plots of Zn and Zn-composite coatings

Table 3. Electrochemical impedance data

Substrates	**R_s (Ωcm^2)**	**R_{coat} (Ωcm^2)**	**Q_{coat} (µF)**	**n**	**R_{ct} (Ωcm^2)**	**Q_{dl} (µF)**	**n**	**RP (Ωcm^2)**
Zn coated	6.006	16.68	356.7	0.61	209.8	4229	0.75	226.48
Zn-1g/L CuO	5.054	413.7	337	0.84	357.1	3860	0.99	770.8
Zn-1g/L NiO-CuO	3.282	372.0	395.4	0.51	673.2	2384	0.96	1045
Zn-2g/L NiO-CuO	3.006	578.8	353.4	0.51	943.2	1694	0.97	1522
Zn-3g/L NiO-CuO	3.240	445.9	369.4	0.52	758.0	1839	0.97	1203

3.2.4. Surface Morphology of generated Zn and Zn-composite coatings

Fig. 11(a), (b) and (c) demonstrate the SEM images of Zn and Zn-composite coating samples respectively. Surface morphology of zinc coating generated from solution without nanoparticles is shown in Fig. 11(a) which showed irregular hexagonal shaped morphology. The addition of nanoparticles to the zinc bath created more nucleation sites for deposition of zinc and reduces the crystal growth formation thus resulted the uniform surface structure compare to pure zinc coating [39].

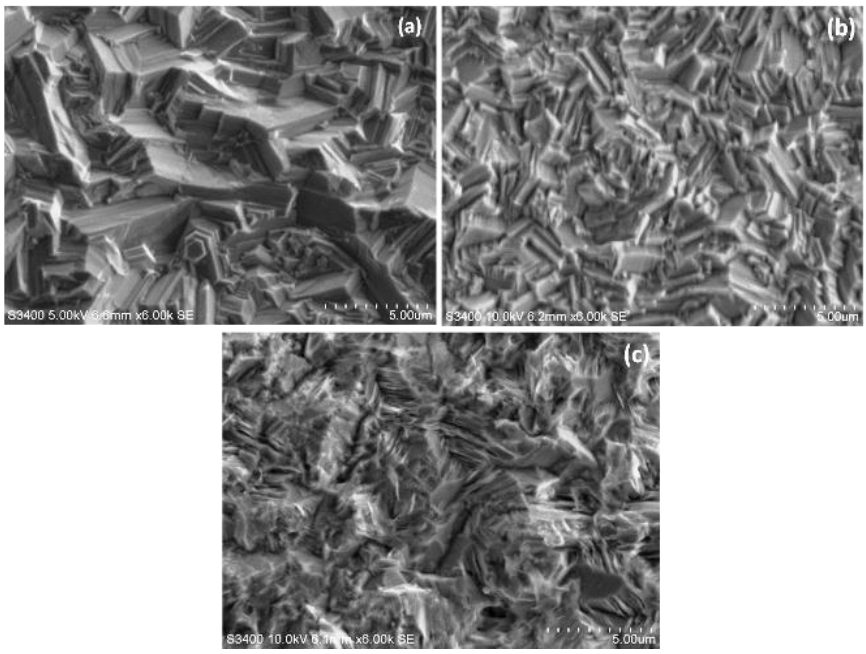

Fig. 11. SEM images of (a) Zn coating (b) Zn-CuO (c) Zn-NiO-CuO

The size of the NiO-CuO nanoparticles was smaller compared to pure CuO hence the inclusion of NiO-CuO into the zinc matrix creates more nucleation sites than CuO nanoparticles and decreased the growth of the crystal. Because of this, NiO-CuO incorporated zinc coated surface shown in Fig. 11(b) obtained more uniformly distributed grain surface than Zn-CuO composite coating. The images of both composite coatings illustrated that the nanoparticles dispersed uniformly in zinc matrix during the deposition process and hence decreased the grain size compared to pure zinc coating. Fig. 12(a), (b) and (c) showed corrosion morphology of Zn and Zn-composite coatings which were subjected to electrochemical corrosion studies in 3.5% NaCl. The more corrosion product formation has been observed in pure Zn coating and lesser corroded morphology was exhibited by Zn-NiO-CuO deposit than Zn-CuO. Compare to CuO nanoparticles, NiO-CuO embedded Zn deposit permits less corrosion reaction towards aggressive media and performed excellent corrosion resistance property revealed by corrosion morphology shown in Fig. 12(c).

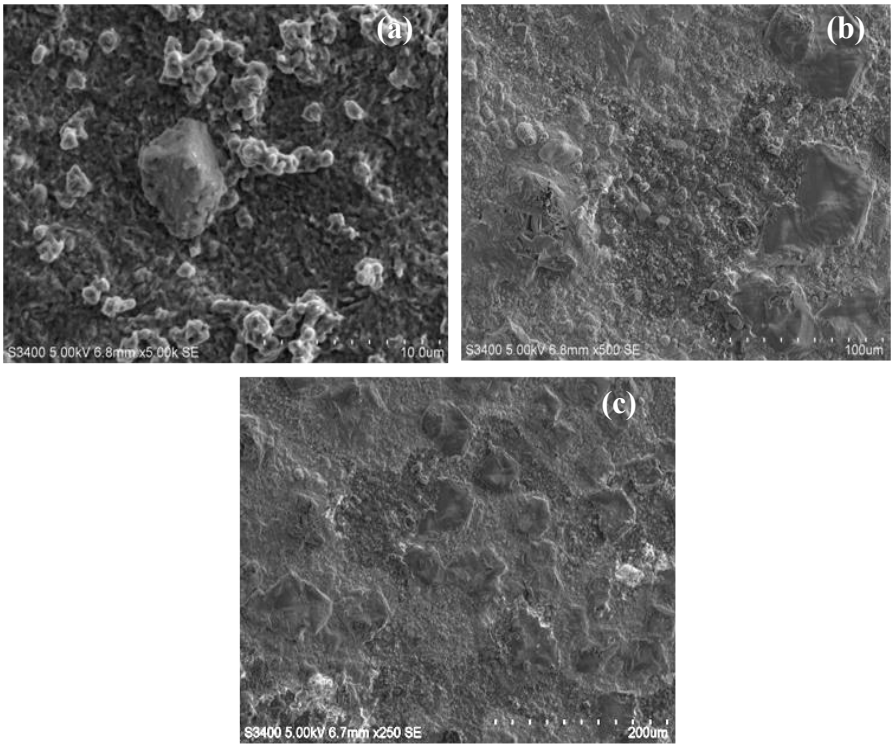

Fig. 12. Corrosion morphology of (a) Zn (b) Zn-CuO (c) Zn-NiO-CuO deposits after corrosion test 3.5% NaCl solution

4. CONCLUSION

The CuO and NiO-CuO nanoparticles have been prepared by co-precipitation method and were successfully incorporated in generating Zn-composite coating on mild steel by electroplating. The XRD study revealed that the smaller crystallite size of NiO-CuO nanoparticles than CuO was noticed. SEM image of CuO nanoparticles showed small spindle shaped like structure and the spherical shaped morphology was observed in NiO-CuO nanoparticles. The EDS analysis showed that the prepared nanoparticles were free from impurities. The –OH group was detected in the FTIR spectra of nanoparticles. The fabricated Zn-NiO-CuO composite showed good anticorrosive property than Zn-CuO and pure Zn coating which has been confirmed by the results of corrosion studies obtained by OCP measurement, Tafel and electrochemical impedance spectroscopy. The morphological analysis of the coatings was in good agreement with the electrochemical corrosion studies.

Acknowledgment

The authors thank Department of Chemistry, Kuvempu University, Karnataka, India for providing lab facilities to carry out the present work. And also UGC-New Delhi, Government of India for providing UGC-BSR Fellowship.

REFERENCES

[1] S. M. A. Shibli, B. N. Meena, and R. Remya, Surf. Coat. Technol. 262 (2014) 210.
[2] P. SungMo, and S. MinYoung, J. Ind. Eng. Chem. 21 (2015) 1258.
[3] Z. Changlu, L. Xin, X. Zhong, L. Juan, and Z. Yanfeng, Corros. Sci. 80 (2014) 269.
[4] S. John, J. Abraham, J. J. Ajith, and B. Narayana, Prog. Org. Coat. 84 (2015) 28.
[5] K. Vathsala, T. V. Venkatesha, B. M. Praveen kumar, and K. O. Nayana, Engineering 2 (2010) 580.
[6] M. K. Punith Kumar, and T. V. Venkatesha, J. Chem. Pharm. Res. 5 (2013) 253.
[7] S. Ghaziof, and W. Gao, J. Alloy. Comp. 654 (2016) 51.
[8] A. P. I. Popoola, O. S. I. Fayomi, V. S. Aigbodion, M. Abdulwahab, Int. J. Adv. Manuf. Technol. 85 (2016) 1419.
[9] R. C. Rathod, S. S. Umare, V. K. Didolkar, B. H. Shambharkar, and A. P. Patil, Trans Indian Inst. Met. 66 (2013) 97.
[10] B. M. Praveen, and T. V. Venkatesha, Appl. Surface Sci. 254 (2008) 2418.
[11] V. Adriana, V. Simona, P. Aurel, B. Caius, and M. Liana Maria, J. Appl. Electrochem. 40 (2010) 1519.
[12] O. S. I. Fayomi, and A. P. I. Popoola, Acta Metall. Sin. (Engl. Lett) 28 (2015) 521.
[13] K. Vathsala, and T. V. Venkatesha, Appl. surface sci. 257 (2011) 8920.
[14] S. Ranganatha, T. V. Venkatesha, K. Vathsala, and M. K. Punith kumar, Surface Coat. Technol. 208 (2012) 64.
[15] K. G. Chandrappa, T. V. Venkatesha, K. O. Nayana, and M. K. Punithkumar, Mater. Corros. 63 (2012) 445.
[16] O. Hammami, L. Dhouibi, P. Berc, E. M. Rezrazi, and E. Triki, Int. J. Corros. 2012 (2012) 8pages.
[17] K. G. Chandrappa, and T. V. Venkatesha, Mater. Corros. 64 (2013) 831.
[18] N. Malatji, and A. P. I. Popoola, Int. J. Electrochem. Sci. 10 (2015) 3988.
[19] O. S. I. Fayomi, A. P. I. Popoola, and O. E. Olorunniwo, Int. J. Adv. Manuf. Technol. 87 (2016) 389.
[20] A. P. I. Popoola, V. S. Aigbodiona, and O. S. I. Fayomi, Surface Coat. Technol. 306 (2016) 448.
[21] S. Ramya, G. Viruthagiri, R. Gobi, N. Shanmugam, and N. Kannadasan, J. Mater. Sci. Mater. Electron. 27 (2016) 2701.
[22] S. E. Anita, and K. Dae Joon, Nanoscale Res. Lett. 7 (2012) 70.
[23] S. Al-Amri, M. S. Ansaril, S. Rafique, M. Aldhahril, S. Rahimuddin, A. Azaml, and A. Memic, Current Nanosci. 11 (2015) 191.
[24] A. S. Abd El-Aziz, M. Mohamed, W. Abd El, A. Soliman, and N. G. Mohamed, Nanosci. Nanoeng. 2 (2014) 17.
[25] B. Nisha, and P. Jeevanandam, J. Alloy. Comp. 537 (2012) 232.

[26] S. G. Hosseini, and R. Abazari, RSC Adv. 5 (2015) 96777.
[27] P. Kankani, S. Sineenart, M. Wanichaya, and P. Wisanu, Energy Proced. 34 (2013) 740.
[28] H. Mohammad, S. Hossein, G. Davood, and S. N. Masoud, J. Mater. Sci. Mater. Electron. 27 (2016) 2718.
[29] S. Ranganatha, T.V. Venkatesha, K. Vathsala, Appl. Srf. Sci. 256 (2010) 7377.
[30] Z. Abdel Hamid, S.M. El-Sheikh, J. Metallurg. Eng. 2 (2013) 71.
[31] A. Olad, M. Barati, S. Behboudi, Progr. Org. Chem. 74, (2012) 221.
[32] Y. Arthoba naik, T.V. Venkatesha, P. Vasudeva Nayak, Turk. J. Chem. 26 (2002) 725.
[33] C. M. PraveenKumar, T. V. Venkatesha, K. Vathsala, and K. O. Nayana, J. Coat. Technol. Res. 9 (2012) 71.
[34] G. Roventi, G. Giuliani, M. Pisani, and T. Bellezze, Int. J. Electrochem. Sci. 12 (2017) 663.
[35] K. G. Chandrappa, and T. V. Venkatesha, Mater. Corros. 65 (2014) 509.
[36] A. Madhan Kumar, and Z. M. Gasem, Progr. Org. Coat. 78 (2015) 387.
[37] M. K. Punith Kumar, T. V. Venkatesha, M. K. Pavithra, and A. Nithyananda Shetty, Syn. Reacti. Inorg. Met. 42 (2012) 1426.
[38] J. Bonastre, P. Garcés , J.C. Galván, F. Cases, Progr. Org. Coatings. 66 (2009) 235.
[39] K. Vathsala, T.V. Venkatesha, J Solid State Electrochem. 16 (2012) 993.